



HAL
open science

Bringing Conducting Polymers to High Order: Toward Conductivities beyond 10^5 S cm^{-1} and Thermoelectric Power Factors of $2 \text{ mW m}^{-1} \text{ K}^{-2}$

Yuhan Zhong, Vishnu Vijayakumar, Viktoriia Untilova, Mounib Bahri, Laurent Herrmann, Laure Biniak, Nicolas Leclerc, Martin Brinkmann

► To cite this version:

Yuhan Zhong, Vishnu Vijayakumar, Viktoriia Untilova, Mounib Bahri, Laurent Herrmann, et al.. Bringing Conducting Polymers to High Order: Toward Conductivities beyond 10^5 S cm^{-1} and Thermoelectric Power Factors of $2 \text{ mW m}^{-1} \text{ K}^{-2}$. *Advanced Energy Materials*, 2019, 9 (24), pp.1900266. 10.1002/aenm.201900266 . hal-02194240

HAL Id: hal-02194240

<https://hal.science/hal-02194240>

Submitted on 5 Jan 2022

HAL is a multi-disciplinary open access archive for the deposit and dissemination of scientific research documents, whether they are published or not. The documents may come from teaching and research institutions in France or abroad, or from public or private research centers.

L'archive ouverte pluridisciplinaire **HAL**, est destinée au dépôt et à la diffusion de documents scientifiques de niveau recherche, publiés ou non, émanant des établissements d'enseignement et de recherche français ou étrangers, des laboratoires publics ou privés.

Bringing conducting polymers to high order: towards
conductivities beyond 10^5 S/cm and thermoelectric power
factors of $2 \text{ mW}\cdot\text{m}^{-1}\cdot\text{K}^{-2}$

Vishnu Vijayakumar^{1*}, Yuhan Zhong^{1*}, Viktoriia Untilova^{1*}, Mounib Bahri²,
Laurent Herrmann¹, Laure Biniek¹, Nicolas Leclerc³ and Martin Brinkmann¹⁺

(1) Université de Strasbourg, CNRS, ICS UPR 22, F-67000 Strasbourg,
France

(2) Institut de Physique et Chimie des Matériaux de Strasbourg (IPCMS),
UMR7504 CNRS Université de Strasbourg, 23 rue du loess, 67037
Strasbourg Cedex 03, France

(3) Université de Strasbourg, CNRS, ICPEES UMR 7515, F-67087
Strasbourg, France

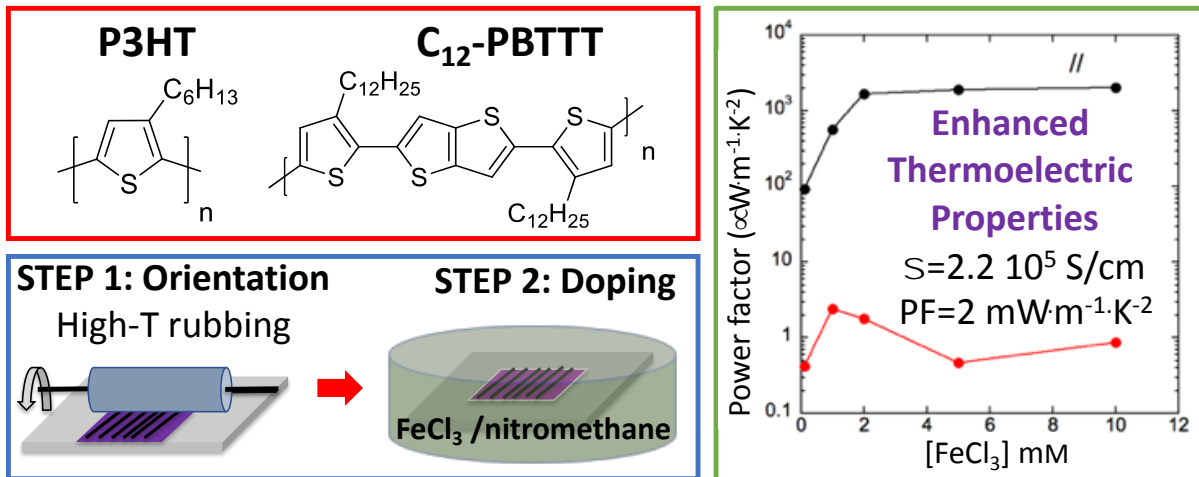
* These authors contributed equally to this work

+ Corresponding authors: martin.brinkmann@ics-cnrs.unistra.fr

Laure.biniek@ics-cnrs.unistra.fr

leclercn@unistra.fr

Figure for Title of Content



An effective design strategy of polymer thermoelectric materials based on structural control in doped polymer semiconductors leads to a substantial improvement of charge conductivity ($>10^5 \text{ S/cm}$) and thermoelectric power factors ($2 \text{ mW}\cdot\text{m}^{-1}\cdot\text{K}^{-2}$). The highly anisotropic conducting polymer films are ideal model systems to investigate the correlations between thermopower S and charge conductivity σ .

Abstract

This study presents an effective design strategy of polymer thermoelectric materials based on structural control in doped polymer semiconductors. The strategy is illustrated for two archetypical polythiophenes e.g. poly(2,5-bis(3-dodecyl-2-thienyl)thieno[3,2-*b*]thiophene) (C₁₂-PBTTT) and regioregular poly(3-hexylthiophene) (P3HT). FeCl₃ doping of aligned films results in charge conductivities up to $2 \cdot 10^5$ S/cm and metallic-like thermopowers similar to iodine-doped polyacetylene. The films are almost optically transparent and show strongly polarized near-infra-red polaronic bands (dichroic ratio > 10). The comparative study of structure-property correlations in P3HT and C₁₂-PBTTT identifies three conditions to obtain conductivities beyond 10^5 S/cm: i) achieve high in-plane orientation of conjugated polymers with high persistence length, ii) ensure uniform chain oxidation of the polymer backbones by regular intercalation of dopant molecules in the polymer structure without disrupting alignment of π -stacked layers and iii) maintain a percolating nano-morphology along the chain direction. The highly anisotropic conducting polymer films are ideal model systems to investigate the correlations between thermopower S and charge conductivity σ . A scaling law $S \propto \sigma^{-1/4}$ prevails along the chain direction but a different $S \propto \ln(\sigma)$ relation is observed perpendicular to the chains, suggesting different charge transport mechanisms. The simultaneous increase of charge conductivity and thermopower along the chain direction results in a substantial improvement of thermoelectric power factors up to $2 \text{ mW m}^{-1} \text{ K}^{-2}$ in C₁₂-PBTTT.

Keywords: Organic Thermoelectrics, Conducting Polymers, Polymer Crystallization, Thin films.

I. Introduction.

Conducting polymers were at the forefront of research in plastic electronics several decades ago and opened the new and vast research field of plastic electronics. A. Heeger, A. G. McDiarmid and H. Shirakawa were among the pioneers in this domain and their success on conducting polymers was recognized by the award of a Nobel Prize in 2000. ^[1] Among all conducting polymers, iodine-doped polyacetylene (PA) demonstrated some of the highest conductivities - up to 10^5 S/cm at room temperature - for stretch-aligned films as well as very high thermoelectric power factors of $1.3 \text{ mW}\cdot\text{m}^{-1}\cdot\text{K}^{-2}$ ^[2-5] However, PA could only be processed in the form of free-standing films several tens of microns in thickness that are difficult to use for TE device fabrication. To alleviate this lack of processing of pure conjugated polymers, alkyl side chains were introduced to design new semi-conducting polymers that are soluble in organic solvents, and thus easily processable via spin-coating, inkjet printing and other solution-based coating methods.^[6,7] With the further control of regioregularity, highly ordered polymer semiconductors (PSCs) with charge mobilities beyond $1 \text{ cm}^2/\text{V}\cdot\text{s}$ ideally suited for OFETs were designed. ^[7] In the subsequent decades, research efforts focused on to the way to fine-tune the electronic properties of the semi-conducting polymers used in the fabrication of Organic Light Emitting Diodes, Field Effect Transistors and Organic Solar Cells.^[8] Chemical engineering helped identify the required structures of conjugated polymers necessary to tune their band gap and/or their absorption spectra to match the solar spectrum.^[9]

Recently, new interest in conducting polymers was triggered by the pioneering work of Crispin et al. on thermoelectric (TE) applications based on the conducting polymer

poly(ethylenedioxythiophene) (PEDOT) doped with tosylate (Tos).^[10,11] Conducting polymers such as PEDOT-Tos have a layered structure of positively charged poly(ethylenedioxythiophene) chains alternating with layers of tosylate anions. (11) PEDOT-Tos shows remarkable thermoelectric properties due to the combination of high charge conductivity, reasonable thermopowers and low thermal conductivity.^[10,11] Despite promising TE properties, the crystallization of PEDOT-Tos in thin films is difficult to control. So far, no simple method is available to either orient in-plane the PEDOT chains or to select the preferential contact plane of crystals on a given substrate. For a large part the synthetic method is to blame: it requires the use of *in-situ* polymerization techniques with a low control over the polymerization process and finally the structure of the polymer thin films. The only improvements in charge transport were obtained via control of secondary crystallization e.g. by using co-solvents such as ethylene glycol that helps extract the non-conducting polystyrene sulfonate from the bulk of the PEDOT-PSS films.^[12,13]

In strong contrast, advanced control of crystallization, crystal orientation and alignment have all been demonstrated for polymer semiconductors (PSCs) such as regio-regular poly(3-hexylthiophene) (P3HT) or poly(2,5-bis(3-dodecyl-2-thienyl)thieno[3,2-*b*]thiophene) (C₁₂-PBTTT) (See Figure 1a).^[18,19] Numerous methods including self-seeded growth, blade-coating, epitaxy or high temperature rubbing help control precisely the crystal dimensions and their orientation in thin films, resulting in diverse morphologies: single crystals, spherulites, aligned crystalline lamellae.^[14-20] It is therefore natural to take profit of the high structural control gained on polymer semiconductors such as P3HT or PBTTT to further improve their charge transport and thermoelectric properties after doping. Doping of thin films of P3HT or PBTTT with fluoroalkylsilanes (FTS) or F₄TCNQ has led to high conductivities typically of the order of a few hundreds to one thousand S/cm.^[21-23] Vapor-phase doping of P3HT and PBTTT with F₄TCNQ leads to conductivities of 12.7 S/cm and

200 S/cm, respectively.^[22,23] Controlled doping of well-crystallized and oriented conjugated polymer can further lead to anisotropic conducting polymer films.^[24] Solution-doping of rubbed P3HT films with F₄TCNQ afforded aligned conducting polymers with conductivities of the order of 22 S/cm whereas vapor phase doping of highly crystalline P3HT afforded 12.7 S/cm conductivities.^[22,24] More recently, the impact of the alkyl side chains on the efficiency of doping, its kinetics and the ultimate TE properties, was demonstrated for the family of PBTTT with alkyl side chains from C₈ to C₁₈.^[25] However, those values remain well below the best conductivities reported for doped polyacetylene (PA) or even PEDOT-Tos.

Is it possible to reach the conductivities of doped PA close to 10⁵ S/cm for oriented films of P3HT or PBTTT (see Figure 1.a) after doping and what limits the ultimate conductivities? To answer these questions, we have investigated the possibility to reach high doping levels in films of P3HT and PBTTT oriented by high temperature rubbing.^[18,24,26,27] The choice of the two polymers is guided by their structural differences in terms of nanomorphology in rubbed thin films: P3HT has a periodic semi-crystalline lamellar morphology whereas C₁₂-PBTTT shows a liquid-crystalline-like structure.^[18,19] The choice of FeCl₃ is motivated by the fact that it is a stronger oxidant than F₄TCNQ.^[28] Accordingly, this manuscript is divided in three parts dealing with: i) the structural and spectroscopic features induced by FeCl₃-doping on aligned P3HT and C₁₂-PBTTT films, ii) the dependence of charge transport and thermopower on [FeCl₃] concentration and iii) the analysis of the S- σ correlations in the oriented films of P3HT and C₁₂-PBTTT.

II. Results.

1) Structural signatures of FeCl₃ doping.

As demonstrated previously for P3HT and F₄TCNQ, the combination of an orientation method such as mechanical rubbing and sequential doping in an orthogonal solvent (See Figure 1) yields highly oriented and crystalline conducting polymer films. The same strategy was applied to P3HT and C₁₂-PBTTT doped with FeCl₃. A drastic change of the film's color from purple to light blue (see Figure 1.c) is observed after doping the polymer films with 10mM FeCl₃ in nitromethane. Polarized Optical Microscopy (POM) shows that doping does not suppress the orientation of the films, even for high FeCl₃ concentrations (10mM) (see Figure 1.d).

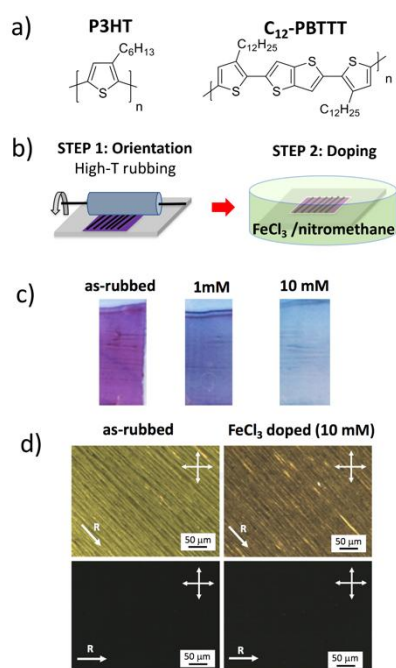


Figure 1. a) Chemical structure of P3HT and C₁₂-PBTTT. b) Schematic illustration of the two step process to prepare oriented conducting thin films combining high temperature rubbing and subsequent doping in a solution of FeCl₃ in nitromethane. c) Illustration of the color change in rubbed C₁₂-PBTTT films (left) upon doping with 1 mM and 10 mM FeCl₃/nitromethane solutions. d) Polarized Optical Microscope images under crossed polarizers showing the high birefringence in the as-rubbed and doped C₁₂-PBTTT films.

The preserved orientation in the doped films is also demonstrated by Transmission Electron Microscopy (TEM). Figure 2 compares the electron diffraction patterns of the pristine and FeCl_3 -doped P3HT and PBTTT oriented films. The electron diffraction (ED) patterns of pristine oriented films indicate that the chain direction is parallel to the rubbing direction R and that crystalline domains are oriented mainly face-on the substrate in C_{12} -PBTTT whereas face-on and edge-on crystals coexist in oriented P3HT films. Both the in-plane orientation and crystal contact plane are maintained after doping for P3HT and C_{12} -PBTTT for the whole range of $[\text{FeCl}_3]$. However, on closer inspection, the ED patterns after doping for $[\text{FeCl}_3] = 10 \text{ mM}$ reveals a loss of crystallinity characterized by a partial loss of higher order equatorial $h00$ reflections, a broadening of the remaining $h00$ and a reduction in the intensity of the meridional 002 reflection.

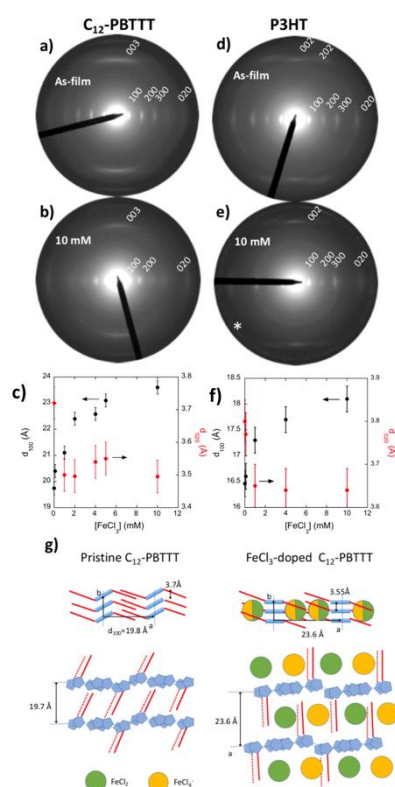


Figure 2. Structure evolution in doped P3HT and C_{12} -PBTTT upon doping with FeCl_3 as obtained by low dose TEM. Electron diffraction patterns of C_{12} -PBTTT before (a) and after (b) doping with 10 mM FeCl_3 . c) Interlayer spacing d_{100} and π -stacking distance versus FeCl_3 concentration in nitromethane for C_{12} -PBTTT films. TEM. Electron diffraction patterns of

C₁₂-PBTTT before (d) and after (e) doping with 10 mM FeCl₃. In (e), the asterisk marks a Scherrer ring from excess FeCl₃ on the surface of the doped P3HT film. f) Interlayer spacing d_{100} and π -stacking distance versus FeCl₃ concentration in nitromethane for P3HT films. (g) Illustration of the structural change induced by FeCl₃ doping for C₁₂-PBTTT ([FeCl₃]=10 mM) that results in the formation of a bimolecular crystal.

As seen in Figure 2.c and 2.f, doping modifies the unit cell parameters of C₁₂-PBTTT and P3HT but to different extents (see also figure S1). For both polymers, the unit cell expands along the alkyl side chain direction (d_{100}) and the π -stacking repeat (020) is reduced, demonstrating that dopant molecules penetrate inside the layers of alkyl side chains of the crystalline phase and that the change in lattice parameters correlate with the amount of incorporated dopants.^[24,25] For both polymers, the interlayer spacing d_{100} increases with [FeCl₃] and saturates for [FeCl₃] approaching 10 mM. A maximum of doping has been reached. d_{100} increases from 19.7 Å (pristine) to 23.6 Å (10 mM) in C₁₂-PBTTT and from 16.4 Å (pristine) to 18.1 Å (10 mM) for P3HT.

For both polymers, doping results in a small decrease of the π -stacking periodicity similar to that observed with F₄TCNQ doping.^[24,25] The main difference between C₁₂-PBTTT and P3HT resides in the evolution of the side chain spacing. In C₁₂-PBTTT, the maximum change in d_{100} is equivalent to 3 CH₂-CH₂ bonds i.e. 3.9 Å whereas in P3HT it is only 1.7 Å. In both cases, the increase of d_{100} is smaller than the 7.4 Å van der Waals diameter of FeCl₄⁻. Even more telling is the variation in unit cell volume ΔV in both cases. Assuming orthorhombic unit cells with two chains per unit cell for both P3HT (a=16.5 Å, b=7.8 Å and c=7.77 Å) and C₁₂-PBTTT (a=19.7 Å, b=7.4 Å, c=13.5 Å), $\Delta V=20-30 \text{ \AA}^3$ for P3HT *versus* $\Delta V=230-250 \text{ \AA}^3$ for C₁₂-PBTTT. Intercalation of small molecules such as phenyl-C₇₁-butyric acid methyl ester (PC₇₁BM) into the structure of PBTTT has been extensively analyzed and modelled.^[29-31] It

has been shown that PC₇₁BM molecules intercalate in the structure of PBTTT and form bimolecular crystals of PC₇₁BM and C₁₄-PBTTT. The bimolecular crystal phase is characterized by an expanded unit cell parameter along the alkyl side chain direction. Since the van der Waals diameter of FeCl₄⁻ (7.4 Å) is below that of PC₇₁BM it is tempting to propose a similar scenario for FeCl₃-doped C₁₂-PBTTT. Comparing the value of ΔV with the molecular volumes of FeCl₂ (42 Å³) and FeCl₄⁻ (69 Å³) suggests that up to four dopant molecules i.e. 2 FeCl₂ and 2 FeCl₄⁻ can be hosted in the unit cell of C₁₂-PBTTT (see Figure 2.g). *This would imply a stoichiometry of one FeCl₄⁻ plus one FeCl₂ per four thiophene rings in a unit cell at saturation (corresponding thus to an atomic ratio S/Fe=2).* Such a stoichiometry is further consistent with that observed in the heavily doped phase of PEDOT:Tos.^[32,33] To confirm this stoichiometry, we further analyzed our samples using EDX – STEM. Figure S2 and S3 (see ESI) shows the elemental analysis in terms of EDX spectra and 2D maps for 5 mM FeCl₃-doped C₁₂-PBTTT and P3HT. First, one can see that there is a uniform distribution of both S and Fe atoms in the doped layers, indicating that doping is uniform in the samples. Second, the EDX spectra help determine the atomic ratio of S and Fe elements. For C₁₂-PBTTT, one obtains a value close of 1.9±0.2 whereas for P3HT it is approximately 2.5±0.2. The S/Fe ratio for C₁₂-PBTTT is in full agreement with the value deduced from the unit cell parameter variation assuming it is related to the uptake of 2 FeCl₄⁻ and 2 FeCl₂. For P3HT, the situation is different as the unit cell expansion is moderate and does not reflect the uptake of dopants. The absence of important unit cell variation in P3HT suggests that the alkyl side chain layers of P3HT can accommodate more readily the intercalation of FeCl₄⁻ and FeCl₂ molecules possibly because the side chains of P3HT are not interdigitated. However, for both polymers, the incorporation of dopants in the layers of alkyl side chains requires a structural reorganization especially when side chains are interdigitated (see the schematic illustration in Figure 2.g). Lattice expansion along the side chains, partial

removal of interdigitation as well as tilting of the backbones and side chains are the potential mechanisms by which the structure of the doped phase can adapt to a given concentration of dopants. It is worth to mention that both the alkyl side chain sublattices of P3HT and of C₁₂-PBTTT are particularly loose and offer the possibility to harbor dopant molecules. Indeed, the areas per alkyl stem are 24.5 Å² for C₁₄-PBTTT and 27 Å² for P3HT (form I). Both values are substantially lower than the 18.4 Å² for the classical polymethylene subcell, indicating that the layers of side chains can indeed host small molecules such as F₄TCNQ, FeCl₄⁻ or FeCl₂.^[24, 25, 34,35]

2) Nanomorphology of doped thin films.

Both C₁₂-PBTTT and P3HT show a coexistence of crystalline and amorphous domains but their nano-morphologies are substantially different as revealed by bright field and HR-TEM. Firstly, bright field TEM shows that only the P3HT films have a characteristic periodic lamellar morphology (see Figure S4 and S5) whereas no such morphology is observed for rubbed C₁₂-PBTTT. This difference is further visible in the HR-TEM images of figure 3. Highly ordered domains of π -stacked polythiophene backbones periodically separated by layers of alkyl side chains containing the dopants appear in the form of fringed patterns with a 17.6 Å periodicity for doped P3HT and 22.5 Å for doped C₁₂-PBTTT ([FeCl₃] = 4 mM). The ordered domains have very different lengths of planarized chain segments for both polymers: 50-100 nm for C₁₂-PBTTT and 10-15 nm for P3HT. These differences in nano-morphologies are related to different persistence lengths of the two polymer chains: 3 nm for P3HT versus 9 nm for C₁₂-PBTTT.^[36,37] Accordingly, in strong contrast to the periodic semi-crystalline lamellar structure of P3HT, C₁₂-PBTTT displays rather a liquid-crystal-like morphology with extended planarized chain segments along the chain direction (see illustration in Figure 3.b

and 3.e). As a result, the connectivity between ordered domains is far better along the chain direction in C_{12} -PBTTT films (see illustration in figure 3.b and 3.d). As seen hereafter, these different nano-morphologies impact the ultimate conductivities of doped oriented films.

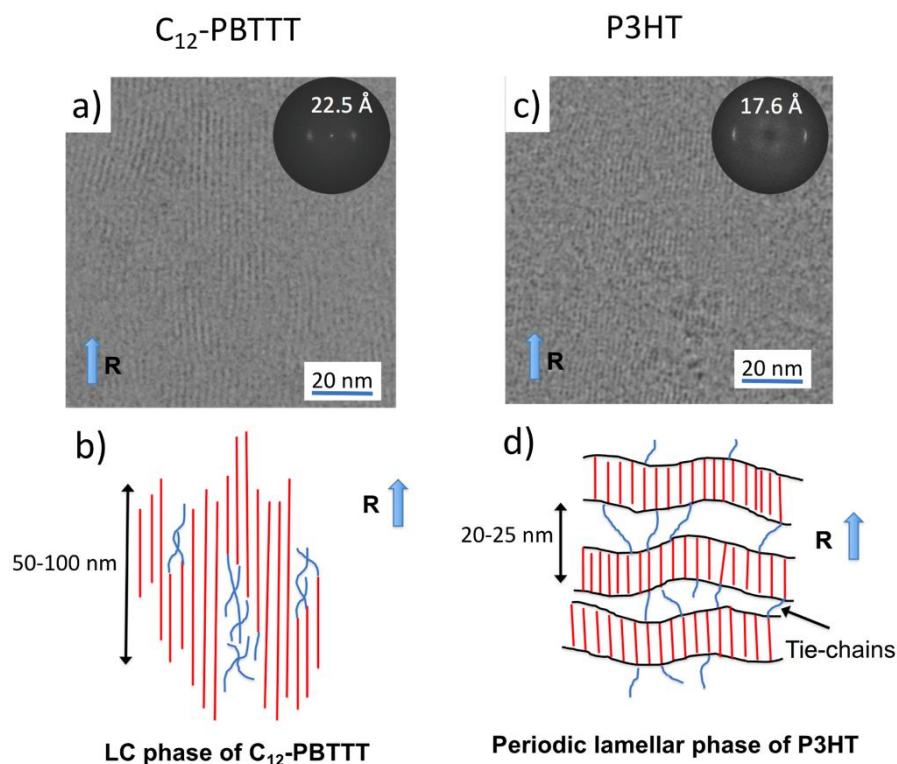


Figure 3. Low dose HRTEM image of $FeCl_3$ -doped C_{12} -PBTTT (a) and P3HT (c) films aligned by high temperature rubbing ($[FeCl_3] = 4 \text{ mM}$). The insets correspond to the Fast Fourier Transforms. Schematic illustration of the nanomorphology in the LC phase of C_{12} -PBTTT (b) and the semi-crystalline lamellar morphology of P3HT (d).

3) Spectroscopic signatures of doping.

TEM has shown that the amount of $FeCl_3$ incorporated in the crystals of C_{12} -PBTTT and P3HT depends on the concentration $[FeCl_3]$. This trend is further supported by Polarized UV-vis-NIR spectroscopy that helps visualize the level of chain oxidation versus $[FeCl_3]$ (see Figure 4). Increasing the doping concentration results in a corresponding increase of the polaronic features P1 and P2 and a decrease of the neutral polymer absorption (N). For both

polymers, the NIR absorption bands P1 and P2 are polarized parallel to the alignment direction R and the films are strongly birefringent under the polarizing microscope. Most remarkably, the P3HT and PBTTT films doped at 10 mM exhibit a spectrum without significant contribution of the original neutral polymer (1-2%), suggesting an oxidation level of the polymer backbones similar to that of PEDOT-PSS (30-40%).^[10] As a result, the films doped with 10 mM FeCl₃ are almost optically transparent with a light blue color similar to PEDOT:PSS (excess FeCl₃ gives rise to a small band at 374 nm).^[38] The presence of the P2 band indicates also that the regime of pure bipolaron formation is not attained for [FeCl₃]= 10 mM (for a nondegenerate ground-state polymer, the P2 transition is forbidden for the bipolaron.^[39]) P1 and P2 are more red-shifted in C₁₂-PBTTT than in P3HT: $\lambda_{\text{max}}(\text{P2}) = 809$ nm for P3HT and 854 nm for C₁₂-PBTTT. Although the position of the P1 peak cannot be observed directly and lies beyond 2500 nm, the slope of the absorbance curve at 2500 nm indicates that the P1 peak is also substantially more red-shifted for C₁₂-PBTTT than for P3HT. Positions of polaronic features are determined by the extent of delocalization and/or crystalline perfection.^[40,41] Hence the red-shifted polaron bands in C₁₂-PBTTT suggest a larger polaron delocalization length relatively to P3HT. This is consistent with the larger extension of aligned and planarized chain segments observed by HR-TEM in C₁₂-PBTTT (see Figure 3).

Typically, C₁₂-PBTTT films doped with 10 mM FeCl₃ have a dichroic ratio of the P2 and P1 band of 10.6, which is very close to 10.8 of undoped C₁₂-PBTTT. These similar values confirm that FeCl₃ doping does not alter substantially the orientation of the C₁₂-PBTTT chains. For oriented P3HT films, the situation is different: the dichroic ratios of the P1 and P2 bands decreases with increasing [FeCl₃] (see Figure S6). This loss of orientation is possibly related to the loss of both alignment and crystallinity upon intercalation of dopant molecules. This is consistent with the decreased intensity of ED reflections and the loss of vibronic

structure in the absorption of the non-doped phase (N). Interestingly, UV-vis spectra for POL \perp R (see Figure 4) indicate that the amorphous fraction of P3HT and C₁₂-PBTTT is also doped with FeCl₃. Indeed, upon doping with increasing [FeCl₃], the absorption band of the amorphous phase (at 526 nm in C₁₂-PBTTT and 506 nm in P3HT, see Figure S7) progressively disappears. This result is at variance with the case of F₄TCNQ-doped films for which no evidence for doping of the amorphous domains was seen by polarized UV-vis spectroscopy (See Figure S8).^[24] The fact that both crystalline and amorphous phases are doped with FeCl₃ explains, at least in part, the higher overall conductivity relatively to F₄TCNQ.^[24]

Comparison with F₄TCNQ-doped films indicates that the doping level achieved with FeCl₃ is substantially larger. In particular, the remaining proportion of neutral C₁₂-PBTTT and P3HT is much lower (only a few percent) for FeCl₃ with respect to F₄TCNQ.^[16] Following the work by Miller et al., the high oxidation levels at saturation of C₁₂-PBTTT and P3HT upon doping with FeCl₃ could reflect a higher dopant miscibility as compared to F₄TCNQ.^[29] Moreover, the spherical shape of the FeCl₄⁻ anions may also favor a closer proximity of the dopant to the polymer backbone as compared to the rod-like F₄TCNQ whose long axis tends to align parallel to the alkyl side chains i.e. in a plane perpendicular to the polymer backbone.^[24,25] As seen hereafter, the higher overall oxidation of P3HT and C₁₂-PBTTT chains achieved upon FeCl₃ doping accounts for the improved charge conductivities.

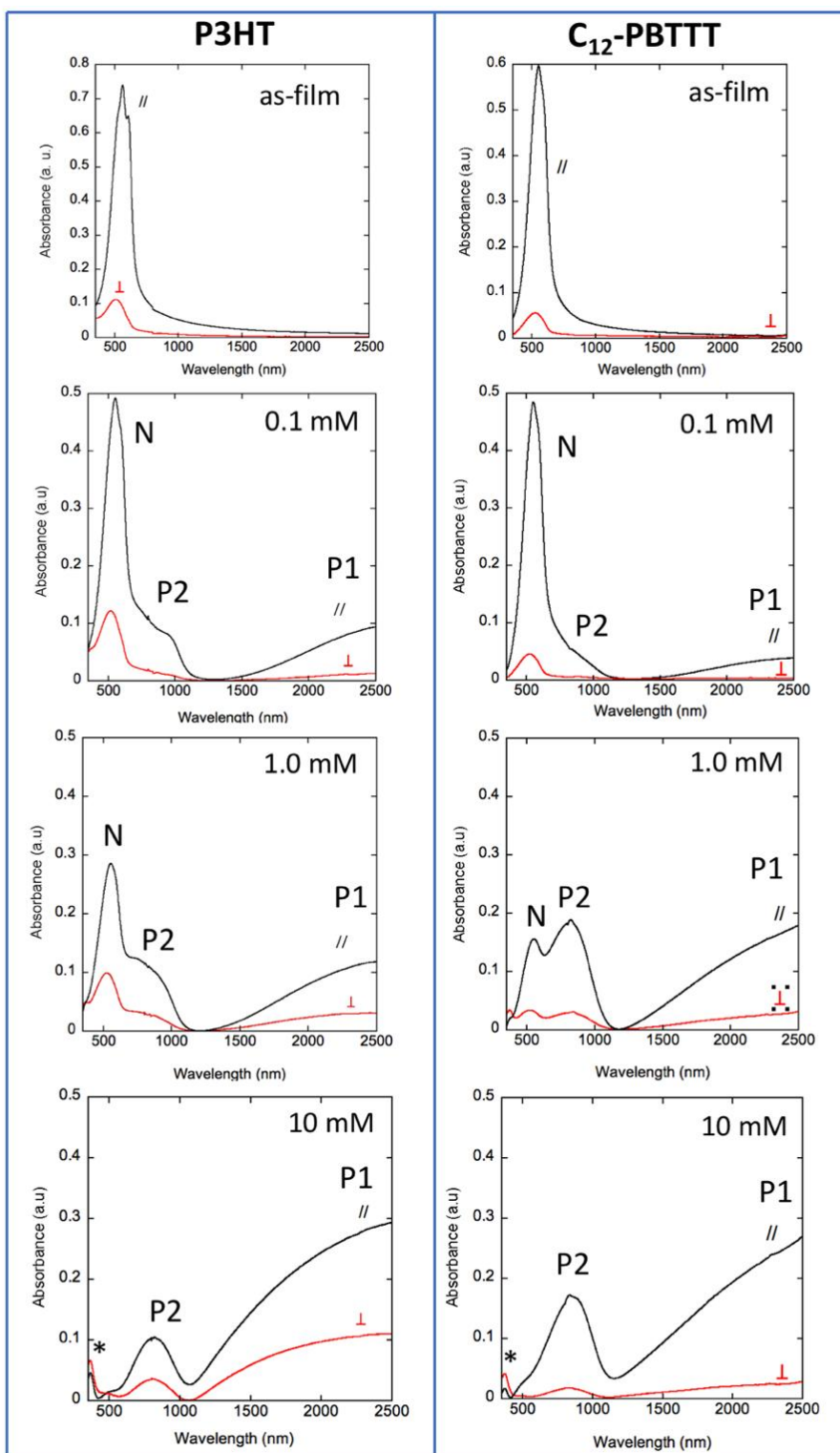


Figure 4. Evolution of the polarized UV-vis-NIR spectrum in oriented P3HT and C₁₂-PBTTT thin films prepared by high temperature rubbing and subsequently doped in solution of FeCl₃/nitromethane of increasing concentration. The light polarization is parallel (//) to the rubbing direction or perpendicular to (⊥). The asterisk highlights the absorption peak of the excess FeCl₃ present on the film surface.

4) **Anisotropy of charge transport.**

As demonstrated in the previous section by TEM and UV-vis-NIR spectroscopy, the proportion of oxidized *versus* neutral chains in the oriented P3HT and C₁₂-PBTTT films can be tuned by adjusting [FeCl₃] while maintaining the high level of in-plane orientation. This gives a handle to control the charge carrier density in the oriented films and to determine its impact on anisotropic charge transport and TE properties. Therefore, a sequential doping protocol was used to probe the changes in charge conductivity and thermopower on a given oriented film sample: the same oriented film was doped in successive steps with a solution of FeCl₃/nitromethane of increasing concentration. This alleviates all issues related to differences in morphology and structure of the rubbed samples that would result in a scattering of the charge conductivity values σ and Seebeck coefficients S . Figure 5 shows the evolution of σ and S *versus* FeCl₃ concentration for P3HT and C₁₂-PBTTT oriented films that were sequentially doped with FeCl₃ solutions of increasing concentration. Table 1 collects the highest values of conductivity and power factors for both doped polymers and corresponding values from the literature for iodine-doped PA.

Upon doping, both P3HT and C₁₂-PBTTT show a strong increase of conductivity with a saturation at higher FeCl₃ concentration (for both // and \perp directions). In the aligned C₁₂-PBTTT films, the conductivity increases by several orders of magnitude from 150 S/cm at 0.1 mM to $2.2 \cdot 10^5$ S/cm at 5 mM. The highest conductivities of C₁₂-PBTTT surpass the 10^5 S/cm reported for stretch-oriented bulk films of polyacetylene doped with iodine.^[4] However, it is worth to note that it is necessary to realize a progressive doping with increasing dopant concentration to reach such large conductivities. Indeed, C₁₂-PBTTT films doped directly with a 10 mM solution reach only a 10^4 S/cm conductivity. As a matter of fact, PBTTTs with shorter or longer alkyl side chains showed also very high conductivities (see Table SII) albeit

below those of C₁₂-PBTTT. This specificity of C₁₂-PBTTT was previously noted in the case of F₄TCNQ-doped PBTTTs and reflected a higher doping level for this polymer.⁽²⁵⁾

For the highly conducting C₁₂-PBTTT films, one can estimate the charge carrier density based on the structural data indicating that the unit cell contains two FeCl₄⁻ anions per unit cell, which translates to a maximum of two charge carriers per unit cell i.e. a carrier density of approx. $9 \cdot 10^{20} \text{ cm}^{-3}$.^[42] This value is larger than the $0.3\text{-}0.95 \cdot 10^{20} \text{ cm}^{-3}$ reported for FTS-doped PBTTT.^[43] However, the present result appears consistent in view of the UV-vis-NIR results indicating full oxidation of the C₁₂-PBTTT backbone contrary to the FTS-doped PBTTT that showed a substantial amount of neutral polymer chains and an oxidation level of only 3.5-11%.^[43]

As for P3HT, alignment improves substantially the conductivity from 63 S/cm in non-oriented FeCl₃-doped P3HT films to 570 S/cm along the rubbing direction in oriented films (for [FeCl₃] = 5mM).^[38] The anisotropies of charge conductivity are much larger in C₁₂-PBTTT than in P3HT ($\sigma_{//}/\sigma_{\perp}=70$ for C₁₂-PBTTT and 12 for P3HT). This difference is partly due to different film structures. As shown by TEM, the rubbed C₁₂-PBTTT films have a dominant face-on orientation whereas P3HT has a mixture of edge-on and face-on oriented domains. As a consequence, σ_{\perp} is essentially probed along the insulating C₁₂ side chains of C₁₂-PBTTT whereas transport along π -stacking and side chains coexist in P3HT films. As an alternative explanation, the reduced anisotropy of the charge conductivity in P3HT could be due to the loss of orientation/crystallinity and/or to the doping of amorphous zones for increasing [FeCl₃] as suggested by polarized UV-vis spectroscopy.

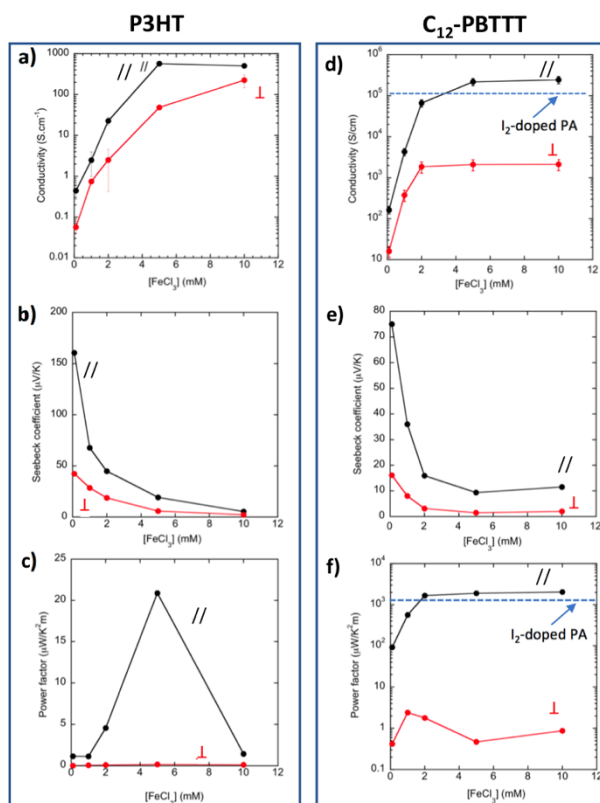


Figure 5. Variation of the charge conductivity σ (a and d), Seebeck coefficient S (b and e) and power factor PF (c and f) as a function of increasing $FeCl_3$ concentration for doped P3HT and C_{12} -PBTTT oriented films. σ , S and PF are measured along the rubbing direction ($//$) and perpendicular to it (\perp). The lines are guide to the eye. The blue dotted lines in d) and e) show the typical values of conductivity and power factors reached for PA doped with iodine, respectively.

As a rule, the maximum conductivity of doped P3HT films is always below that of C_{12} -PBTTT. It does not reflect a difference in the degree of in-plane orientation since both polymers have similar high dichroic ratios prior to doping. It is also not due to different doping levels since the spectroscopic features for 10 mM-doped films of P3HT and C_{12} -PBTTT are almost identical. The lower conductivity of doped P3HT must thus reflect intrinsic charge transport limitations related to its semi-crystalline periodic lamellar structure. In doped P3HT films, charges must necessarily channel through the less conductive amorphous zones that harbor chain ends and chain folds, hence, lowering the macroscopic

conductivity $\sigma_{//}$. In the liquid crystal-like structure of C₁₂-PBTTT, more effective percolation between ordered domains of highly aligned chains in the rubbing direction (see HRTEM image in Figure 2) results in a larger conductivity $\sigma_{//}$. Even in the direction perpendicular to the rubbing, C₁₂-PBTTT films display particularly high conductivities of ~ 2100 S/cm that are close to those observed in non-oriented FTS-doped C₁₄-PBTTT.^[21] This indicates that the conductivity measured in non-oriented PBTTT samples is essentially limited by the charge transport perpendicular to the chains. Achieving such high conductivities in doped C₁₂-PBTTT on a macroscopic scale implies also that charges must be transported quite effectively between the well doped and ordered domains seen in HRTEM. Charge tunneling between highly conducting domains is the mechanism invoked in a granular metal model of Sheng to account for comparably high conductivities in heavily-doped PA.^[44] In strong contrast, in P3HT, the large extension of amorphous interlamellar zones will hamper tunneling between doped crystalline regions and limit the macroscopic conductivity.

5) Anisotropy of thermopower and power factor.

As seen in Figure 5.b and 5.e, the thermopower variation with dopant concentration is inverse to that of charge conductivity: both Seebeck coefficients $S_{//}$ and S_{\perp} decrease with [FeCl₃]. In all samples, the thermopower probed along the chain direction is larger than that measured perpendicular: $S_{//} > S_{\perp}$.^[23] The anisotropy factor of the Seebeck coefficient $S_{//}/S_{\perp}$ tends to decrease with increasing FeCl₃ concentration for both polymers. The anisotropies are higher for C₁₂-PBTTT (4.6) than for P3HT (2.4). Overall, as observed previously for F₄TCNQ-doped P3HT, the anisotropy in thermopower is always smaller than that of the charge conductivity.^[24,25]

Table 1. Thermoelectric characteristics of the FeCl₃-doped oriented films of C₁₂-PBTTT and P3HT and comparison with stretch-oriented iodine-doped PA (3).

Sample	P3HT [FeCl ₃]=5 mM	C ₁₂ -PBTTT [FeCl ₃]=5 mM	I ₂ -doped PA (ref. 3)
$\sigma_{//}$ (S/cm)	570±100	(2.2±0.5)10 ⁵	6·10 ⁴
σ_{\perp} (S/cm)	48±20	2100±300	-
$S_{//}$ (μV/K)	5.4±0.5	9.4±0.5	15
S_{\perp} (μV/K)	2.3±0.5	1.5±0.5	-
Power factor PF _{//} (μW·m ⁻¹ ·K ⁻²)	21±6	1944±626	1350

The samples with highest conductivities have very small thermopowers (see Table 1). For instance, the rubbed C₁₂-PBTTT sequentially doped with 5 mM FeCl₃/nitromethane have $\sigma_{//}=2.2 \cdot 10^5$ S/cm and $S_{//}=9.4\pm 0.5$ μV/K. Their Seebeck coefficients measured perpendicular to the alignment are even smaller with $S_{\perp}=1.5 \pm 0.5$ μV/K. Such low thermopowers are characteristic of metals.^[45] For comparison, oriented films of PA doped with iodine have $S_{//}=15$ μV/K.^[3,4]

At this point we focus on the origin of the anisotropy of the thermopower S in oriented doped films of P3HT and C₁₂-PBTTT. The present situation bears similarity with the case of doped oriented PA fibers that show $S_{//}/S_{\perp}>1$.^[46,47] Kaiser proposed a heterogeneous model of metallic fibrils separated by electrical barriers to explain this observation.^[46] In doped PA, semi-conducting barriers alternate with metallic domains and modulate the thermopower and its anisotropy. The situation is similar for doped oriented P3HT and C₁₂-PBTTT. Indeed, HRTEM evidences the semi-crystalline morphology of doped P3HT and C₁₂-PBTTT with a clear coexistence of highly ordered domains and amorphous interlamellar zones. Moreover, it is known that the charge conductivity is higher in crystalline *versus* amorphous domains of doped P3HT (typically a few S/cm are obtained in F₄TCNQ-doped regio-regular P3HT *versus*

0.01 S/cm in regio-random amorphous P3HT). (22) This difference in charge transport between amorphous and crystalline domains must translate into a corresponding difference of the thermopower S_a and S_χ for amorphous and crystalline domains, respectively, with $S_a > S_\chi$. Accordingly, the semi-crystalline morphology of oriented conducting polymer films can be analyzed by using a heterogeneous material model similar to that proposed for doped PA.

When the temperature gradient ΔT is oriented parallel to the rubbing, it is distributed over a succession of crystalline and disordered (amorphous) domains connected in series. We consider that the sample consists of a fraction χ of crystalline domains. The crystalline domains are characterized by an average temperature gradient ΔT_χ (along the chain direction) and disordered/amorphous domains by an average temperature gradient ΔT_a . We also assume that the heat current flows along the same path as the charges, so that the temperature gradients across crystalline and amorphous domains are proportional to their thermal resistances ($\Delta T_\chi \propto W_\chi$ and $\Delta T_a \propto W_a$ with W_χ and W_a the thermal resistances of crystalline and amorphous domains, respectively). Hence, the Seebeck coefficient in the rubbing direction $S_{//}$ can be written as: ^[46]

$$S_{//} = \alpha S_\chi + (1-\alpha) S_a \quad (1)$$

Where α is given by:

$$\alpha = \frac{\chi W_\chi}{\chi W_\chi + (1-\chi) W_a} \quad (2)$$

In the case of P3HT, the crystallinity χ is determined by the rubbing temperature and is close to 50% for $T_R = 200^\circ\text{C}$.^[26] In semi-crystalline polymers such as polyolefins, the thermal resistance of crystalline lamellae along the chain direction W_χ is small whereas the one perpendicular to the chains is significantly larger and comparable to that of the amorphous phase i.e. $W_\chi \ll W_a$.^[48] This implies $S_{//} \approx S_a$ i.e. the Seebeck coefficient $S_{//}$ is dominated by the contribution from the doped amorphous and less conducting phase.

Let us now consider what happens when the temperature gradient is oriented perpendicular to the chain direction. In this situation, crystalline and disordered zones are put in parallel along the temperature gradient and charges are short-circuited through the most conductive domains i.e. along the crystalline domains. As seen in TEM of the rubbed 180°C P3HT sample, the crystalline lamellae make a quite continuous conduction path given their lateral extension perpendicular to the rubbing direction (several hundreds of nm) and the way such lamellae are interconnected. Accordingly, charges will be tunneled out of the sample within the crystalline domains in the direction perpendicular to the rubbing and this implies that the observed Seebeck coefficient S_{\perp} is dominated by that of the most conductive lamellae and not by the disordered (amorphous) domains. This implies that $S_{\perp} \approx S_{\chi}$. As a consequence, the Seebeck coefficient anisotropy becomes $S_{//}/S_{\perp} \approx S_a/S_{\chi} > 1$.

The present analysis indicates that a nanostructured morphology in conducting polymers such as doped P3HT or PBTTT that results in a modulation of electronic properties can be beneficial in oriented films since both the thermopower $S_{//}$ and the conductivity $\sigma_{//}$ are increased in the direction of polymer chains. It is important to recall that one major strategy to improve TE properties in inorganic systems is also based on material nano-structuring. Indeed, the objective of nano-structuring inorganic materials such as Bi_2Te_3 is to break the heat transport in the materials through enhanced scattering of phonons at multiple interfaces between domains without breaking charge transport.^[49]

The resulting power factors for the most conductive C_{12} -PBTTT films are very high and can reach values close to $1.94 \text{ mW}\cdot\text{m}^{-1}\cdot\text{K}^{-2}$, a value slightly larger than for I_2 -doped PA ($1.35 \text{ mW}\cdot\text{m}^{-1}\cdot\text{K}^{-2}$).^[3] Such power factors are quite large compared to those of non-oriented films of C_{12} -PBTTT doped with F_4TCNQ from the vapor phase ($0.1 \text{ mW}\cdot\text{m}^{-1}\cdot\text{K}^{-2}$). The combination of orientation and a higher oxidation of the C_{12} -PBTTT polymer after FeCl_3 doping accounts for the remarkable power factors obtained in rubbed thin films. Previous UV-vis studies indicate

that a high proportion of neutral polymer chains is present in oriented P3HT and C₁₂-PBTTT films after doping with F₄TCNQ. This implies a high proportion of semi-conducting chain segments and domains that prevents reaching similarly high conductivities as for FeCl₃ doping.

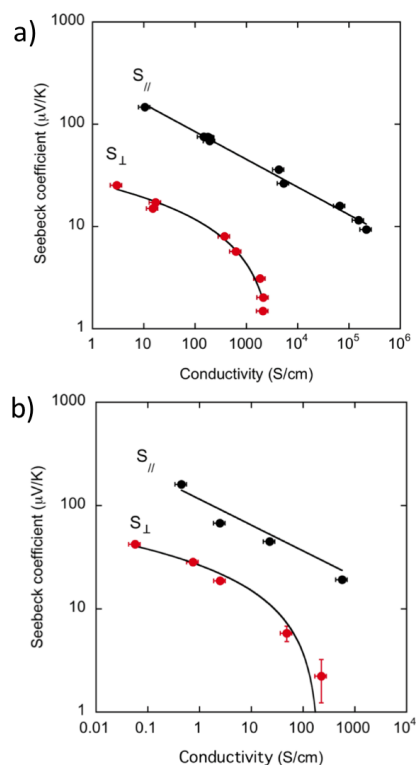


Figure 6. Correlation between thermopower S and charge conductivity s in highly oriented thin films of a) C₁₂-PBTTT ($T_R=125^\circ\text{C}$) and b) P3HT ($T_R=180^\circ\text{C}$) doped with FeCl₃. // and \perp refer to the direction of the measurements respectively parallel and perpendicular to the chain direction. The full lines correspond to the results of the fit using a scaling law $S_{//} \propto \sigma^{-1/4}$ and $S_{\perp} \propto -\ln(\sigma)$ (see text).

6) Correlations between thermopower and charge conductivity in oriented conducting polymer films.

Kang and Snyder have recently demonstrated that details of microscopic charge transport can appear through the correlations between S and σ .^[50] A general theoretical frame relating to the $S=f(\sigma)$ scaling law was recently proposed by these authors. They predicted a

scaling behavior with an exponent $-1/s$ where s is a function of the charge transport mechanism.^[50] In PEDOT:TOS the S - σ curve is well fit with $s=1$ pointing at a transport mechanism dominated by acoustic phonon scattering. The exponent $-1/3$ with $s=3$ is obtained for a transport mechanism involving scattering of carriers by ionized impurities. From an experimental point of view, Chabinyk et al. showed that S and σ are related via the relation $S \propto \sigma^{-1/4}$.^[51,52] The set of (S, σ) data obtained over a large range of conductivities (1.0-10⁵ S/cm) in this study helps further probe the $S=f(\sigma)$ correlations and its anisotropy especially in a regime of high conductivities ($\sigma > 10^3$ S/cm). This methodology alleviates the experimental difficulties associated with charge carrier determinations in doped films e.g. using AC Hall measurements, especially for such aligned films.

The S - σ plots for directions parallel and perpendicular to the chains are shown in Fig. 6.a and 6.b for C₁₂-PBTTT and P3HT, respectively. For both polymers, the $S = f(\sigma)$ plots show different behaviors parallel and normal to the chain directions. In the direction parallel to the chains (**R**), the correlation between $S_{//}$ and $\sigma_{//}$ is well described by a power law with an exponent $-1/4$. This is consistent with previous results by Chabinyk and coworkers for F₄TCNQ-doped C₁₄-PBTTT.^[51,52] In the direction perpendicular to **R**, both polymers show a deviation from the power law, especially for high values of the conductivity. The conductivity σ_{\perp} is observed to saturate close to 200 S/cm in P3HT and 2000 S/cm in C₁₂-PBTTT. The departure from the scaling law in the case of S_{\perp} - σ_{\perp} can have different origins. First, it could be related to some intrinsic structural change in the films when the doping concentration becomes important. We observe that the dichroic ratio for the P1 band as well as the intensity of the reflections in the ED pattern of doped P3HT films tend to decrease when [FeCl₃] approaches 10 mM. A disordering of the layers of π -stacked backbones may be induced by the introduction of increasing amounts of FeCl₃ in the layers of side chains for both P3HT and

C₁₂-PBTTT. This disordering may account for a “saturation” of the conductivity along the chain direction for high FeCl₃ concentration.

Alternatively, the departure from the power law may indicate a different transport mechanism in the direction perpendicular to the polymer chains. As a matter of fact, attempts to fit the S_⊥-σ_⊥ plot indicate that S_⊥ scales rather well with ln(σ_⊥). A similar dependence was reported by Mateeva et al. for oriented polyaniline films for which the S-σ relation was fitted with the equation:^[53]

$$S_i = \frac{-1}{\beta} \left(\frac{k_B}{e} \right) \ln \left(\frac{\sigma_i}{\sigma_i^{max}} \right) \quad (3)$$

with k_B the Boltzmann constant, e the charge of the electron and β a dimensionless coefficient. *i* refers to the direction either parallel (//) or perpendicular (⊥) to the chain direction.^[53]

When fitted with equation (1), one obtains σ_⊥^{max}=3809 S/cm and β=26.7 for C₁₂-PBTTT and σ_⊥^{max}=211 S/cm and β=17.5 for P3HT. These results clearly indicate different intrinsic limitations in charge transport perpendicular to the chain direction for both polymers: charge transport perpendicular to the chains is larger in C₁₂-PBTTT than in P3HT. Regarding the factor β, previous studies on polyaniline reported β ~ 9 whereas much higher values are obtained in the present case for FeCl₃-doped P3HT and C₁₂-PBTTT. In oriented polyaniline samples, Mateeva et al. observed that equation (1) is verified both parallel and normal to the chain direction (albeit for a reduced domain of conductivities well below that measured in the present case). This is clearly not true for C₁₂-PBTTT and P3HT that both show a power law dependence along the chain direction and an apparent logarithmic dependence perpendicular to the chains. Altogether, these results indicate that the S-σ correlations in C₁₂-PBTTT are different along the chain direction and perpendicular to it, supporting different charge transport mechanisms. Interestingly, the same behavior is observed for F₄TCNQ-doped C₁₂-

PBTTT (Figure S9), indicating that it is apparently independent of the chemical nature of the dopant. The similarity of the behavior for FeCl₃ and F₄TCNQ further supports the fact that the high conductivity in FeCl₃-doped films is not related to a contribution from ionic conductivity that should result in a departure from the $S \propto \sigma^{-1/4}$ scaling law. To the best of our knowledge, it is the first time that such a difference between the S- σ correlations is evidenced along and normal to the chain direction. As a matter of fact, different S- σ correlations along and normal to the chain direction would further explain, at least in part, the large spread in experimental data in reference 49 and 50 as the measurements concern isotropic films for which both contributions parallel and normal to the chain direction can combine to different extents.

III. Conclusion.

Controlling crystallization and orientation of polymer semiconductors prior to doping gives a unique handle over the charge transport and thermoelectric properties of the obtained conducting polymer films. This strategy is versatile and can be applied to numerous doped polymer semiconductors including n-type polymers^[54] or low-bandgap polymers^[55,56] that can be oriented by different methods such as blade-coating, high temperature rubbing or epitaxy and subsequently doped using different types of dopants and doping methods. *Central to this approach is the preservation of high order present in the pristine polymer semiconductors upon doping.* This is possible when the dopants intercalate progressively into the layers of side chains by incremental increase of the dopant concentration in such a way that dopant intercalation preserves orientation and π -stacking of the conjugated polymer backbones. Three conditions are identified to obtain conductivities of 10⁵ S/cm: i) achieve high in-plane orientation of conjugated polymers with a high persistence length, ii) ensure a regular intercalation of dopant molecules in the polymer structure to form bimolecular polymer-

dopant crystals and iii) maintain a percolating nano-morphology along the chain direction e.g. via a liquid-crystal-like morphology (semi-crystalline lamellar morphologies are detrimental). Moreover, using a heterogeneous model approach based on the semi-crystalline structure of the doped and aligned polymer films, we are able to account for the anisotropy of the Seebeck coefficient that is enhanced in the direction of alignment.

Two different charge transport behaviors are evidenced in the directions parallel and normal to the polymer chains: $S_{//} \propto \sigma_{//}^{-1/4}$ prevails in the direction parallel and $S_{\perp} \propto -\ln(\sigma_{\perp})$ in the direction normal to the polymer chains. Regarding TE applications, the combination of effective chain alignment and controlled oxidation by sequential doping helps to reach a record power factor of $2 \text{ mW} \cdot \text{m}^{-1} \cdot \text{K}^{-2}$ that could result in high ZT factors provided the thermal conductivity is well contained along the chain direction. Such a result is important as it sets a new upper limit for the ultimate TE power factor of such conducting polymers, but, it will be essential to further address the important issue of thermal conductivity and its correlation to the charge conductivity to obtain TE polymers with outstanding performances.

Acknowledgments.

Bernard Lotz is gratefully acknowledged for fruitful discussions and careful reading of the manuscript and C. Blanck and M. Schmutz for technical support in TEM. P. Allgayer is acknowledged for technical support with the rubbing machine and N. Zimmermann preparation of pre-patterned device. We thank Ovidiu Ersen for giving us access to the EDX spectroscopy facility on the TEM platform from IPCMS. Financial supports from ANR grant Anisotherm and CNRS grant PEPS Thermobody are acknowledged. VV and VU are grateful for financial support from Idex Attractivité (University of Strasbourg) and IRTG Softmatter / Région Grand'Est, respectively.

IV. Experimental Section.

1) Material and characterization.

P3HT was purchased from Merck whereas C₁₂-PBTTT was synthesized following the detailed procedure described in ref. 19. The macromolecular parameters are collected in Table 2. Sodium polystyrenesulfonate (NaPSS), anhydrous FeCl₃ and solvents (anhydrous nitromethane and ortho-dichlorobenzene) were obtained from Aldrich. All the chemicals were used as received.

Table 2. Macromolecular parameters of the semiconducting polymers used in this study. (Gel permeation chromatography was performed in hot trichlorobenzene versus PS standard)

Polymer	M _n (g/mol)	M _w (g/mol)	PDI
P3HT	24200	43600	1.8
C ₁₂ -PBTTT	26000	45000	1.73

2) Orientation of thin films.

The preparation of oriented P3HT and C₁₂-PBTTT films by high-temperature rubbing followed the protocol described in previous publications.^[19,20] P3HT and C₁₂-PBTTT films were prepared by doctor blading a hot polymer solution (10 mg/ml) in ortho-dichlorobenzene (oDCB) on NaPSS-coated glass substrates at 160°C. The NaPSS films are spin coated (3000 rpm, 10 mg/ml aq) on pre-cleaned glass substrates and serve as sacrificial substrates to float the rubbed films on the pre-patterned devices for Conductivity/Seebeck measurements or on copper grids for TEM analysis. High temperature rubbing was performed by using a homemade set up consisting of a translating hot plate on which the sample is fixed and a

rotating cylinder covered with a microfiber cloth. The films were rubbed at different rubbing temperatures depending on the polymer (125°C for C₁₂-PBTTT and 180°C for P3HT). To determine the film thickness after rubbing, the films were melt-annealed at 350°C under nitrogen in a linkam hot stage (HS-95 controller and LTS420 stage) to randomize the in-plane chain direction and the thickness was extracted from the UV-vis absorbance (See Figure S10).

3) Doping protocol.

All doping experiments were carried out in a glove box (Jacomex) with P_{O₂}< 3 ppm and P_{H₂O}<1 ppm. 10 mM FeCl₃ solutions were prepared by dissolving 8 mg of FeCl₃ in 5 ml anhydrous nitromethane in a glass vial and subsequent dilution yielded the solutions with concentration in the range 0.1 - 5 mM. Doping was done by dipping the oriented polymer film in the dopant solution for 30 s – 1 min until no color change was any more visible. Aging of the FeCl₃-doped films is observed when the samples are placed in ambient (dark). Figure S11 exemplifies the evolution of the UV-vis-NIR absorption spectrum and the sheet resistance when the films are transferred from the glovebox to ambient atmosphere. The clear decrease in polaronic absorption correlates with the increase of sample resistance. Typically, the sample's resistance increases by a factor 5 after one hour in ambient. Therefore, all electrical characterizations were performed in a glovebox whereas UV-vis-NIR measurements were performed within 1-2 min after transfer of the sample to the spectrometer in ambient to avoid substantial dedoping.

3) Thin film characterization.

Structural analysis: TEM: The preparation of the samples for TEM analysis involved three steps: i) floating the oriented polymer films on distilled water and recover them on TEM copper grids, ii) coat the films with a thin amorphous carbon layer using an auto 306 Edwards

evaporator and iii) dope the TEM grids directly in the glove box by dropping 20 μl of FeCl_3 /nitromethane solution on the grid. After 30s, the grids were blotted with a piece of absorbing paper to remove the excess of dopant solution.

To avoid sample ageing upon transfer in ambient atmosphere, the TEM grids were mounted on the TEM sample holder inside the glove box and the holder was then transferred to the TEM in an air-tight container. The samples were only swiftly exposed to air (1-2s) just before introducing the sample holder into the TEM. TEM was performed in the bright field and diffraction modes using a CM12 Philips microscope equipped with an MVIII (Soft Imaging System) Charge Coupled Device camera. Beam exposure was set to a minimum using the low dose system to avoid de-doping under the electron beam that is observed when the same zone is exposed for a prolonged period of time.

STEM-EDX experiments were performed using a Cs-corrected JEOL JEM-2100F microscope operated at 100 keV to avoid dedoping of the films under the beam. Energy Dispersive X-Ray spectroscopy (EDX) mapping was performed using JEOL Silicon Drift Detector (DrySD60GV: sensor size 60 mm^2) with a solid angle of approximately 0.5 srad".

Polarized UV-Vis-NIR absorption: The orientation of the polymer films was probed by UV-Vis-NIR absorption (350-2500 nm) using a Cary 5000 spectrometer with polarized incident light and spectral resolution of 1 nm. The UV-Vis-Nir spectra of the doped polymer film were measured parallel and perpendicular to the rubbing direction R.

4) Electrical conductivity and Seebeck Coefficient.

All devices were fabricated on glass substrates following the conditions described in references 24 and 25. 40 nm-thick gold contacts were prepared by thermal evaporation using

appropriate shadow masks. The contact geometry used for the electrical conductivity and thermopower measurements is described and illustrated in Figure S2 of reference 24. To measure the anisotropy of conductivity and TE properties, the devices consist of two devices oriented along the rubbing direction and two oriented normal to the rubbing direction. The oriented P3HT and C₁₂-PBTTT films prepared by rubbing on NaPSS substrates were floated on distilled water and subsequently recovered on the glass-substrates covered with the gold electrodes. Doping with FeCl₃ was performed on these devices by dipping in the solutions of given concentration.

Four-point-probe measurements of electrical conductivity were performed following the procedure described in detail in reference 24 and 25. A Keithley 2634B sourcemeter and a Lab Assistant Semiprobe station in a Jacomex glovebox under N₂ atmosphere were used to measure all conductivity and Seebeck coefficients. The resistivity ρ was derived from the sheet resistance R following the equation $\rho=1.81Rt$ (consider reference 24 for the determination of the geometrical correction factor). The obtained conductivity values are an average of four devices. For the Seebeck coefficients, a differential temperature method was used i.e. a temperature gradient was established across the sample either along the rubbing direction or normal to it. Details of the experimental setup used to measure the thermopower are given in reference 24.

References

- (1) A. J. Heeger, A. G. MacDiarmid, and H. Shirakawa. *Macromolecules* **2002**, *35*, 1137.
- (2) A. J. Heeger, *J. Phys. Chem. B* **2001**, *105*, 8475.
- (3) Y. Nogami, H. Kaneko, T. Ishiguro, A. Takahashi, J. Tsukamoto and N. Hosoi, *Solid State Communications* **1990**, *76*, 583.

- (4) J. Tsukamoto, A. Takahashi and K. Kawasaki, *Jap. J. appl. Phys.* **1990**, 29, 125.
- (5) Y. W. Park, C. Park, Y. S. Lee, C. O. Yoon, H. Shirakawa, Y. Suezaki and K. Akagi, *Sol. Stat. Comm.* **1988**, 65, 147.
- (6) J. Mei and Z. Bao, *Chem. Mater.* **2014**, 26, 604.
- (7) H. Sirringhaus, P. J. Brown, R. H. Friend, M. M. Nielsen, K. Bechgaard, B. M. W. Langeveld-Voss, A. J. H. Spiering, R. A. J. Janssen, E. W. Meijer, P. Herwig, et al. *Nature* **1999**, 401, 685.
- (8) S. Holliday, J. E. Donaghey and I. McCulloch, *Chem. Mater.* **2014**, 26, 647.
- (9) H. Zhou, L. Yang and W. You, *Macromolecules*, **2012**, 45, 607.
- (10) O. Bubnova and X. Crispin, *Energy Environ. Sci.* **2012**, 5, 9345.
- (11) O. Bubnova, Z. U. Khan, A. Malti, S. Braun, M. Fahlman, M. Berggren and X. Crispin, *Nature Materials* **2011**, 10, 429.
- (12) Q. Wei, M. Mukaida, Y. Naitoh and T. Ishida, *Advanced Materials* **2013**, 25 (20), 2831–2836.
- (13) A. M. Nardes, R. A. J. Janssen and M. A. Kemerink, *Advanced Functional Materials* **18**, 865.
- (14) Brinkmann, M. *Journal of Polymer Science Part B-Polymer Physics* **2011**, 49, 1218.
- (15) M. Brinkmann, L. Hartmann, L. Biniek, K. Tremel and N. Kayunkid, *Macromolecular Rapid Communications* **2014**, 35, 9.
- (16) K. Rahimi, I. Botiz, N. Stingelin, N. Kayunkid, M. Sommer, F. P. V. Koch, H. Nguyen, O. Coulembier, P. Dubois, M. Brinkmann, M.; et al. *Angewandte Chemie-International Edition* **2012**, 51, 11131.
- (17) E. J. W. Crossland, K. Tremel, F. Fischer, K. Rahimi, G. Reiter, U. Steiner and S. Ludwigs, *Advanced Materials* **2012**, 24, 839.
- (18) M. Brinkmann and J.-C. Wittmann, *Advanced Materials* **2006**, 18, 860.
- (19) L. Biniek, N. Leclerc, T. Heiser, R. Bechara and M. Brinkmann, *Macromolecules* **2013**, 46, 4014.
- (20) D. M. DeLongchamp, R. J. Kline, Y. Jung, D. S. Germack, E. K. Lin, A. J. Moad, L. J. Richter, M. F. Toney, M. Heeney and I. McCulloch, *ACS Nano* **2009**, 3, 780.
- (21) C. Y. Kao, B. Lee, L. S. Wielunski, M. Heeney, I. McCulloch, E. Garfunkel, L. C. Feldman and V. Podzorov, *Advanced Functional Materials* **2009**, 19, 1906.

- (22) J. Hynynen, D. Kiefer, L. Yu, R. Kroon, R. Munir, A. Amassian, M. Kemerink, and C. Müller, *Macromolecules* **2017**, *50*, 8140.
- (23) K. Kang, S. Watanabe, K. Broch, A. Sepe, A. Brown, I. Nasrallah, M. Nikolka, Z. Fei, M. Heeney, D. Matsumoto, K. Marumoto, H. Tanaka, S. Kuroda and H. Siringhaus, *Nat Mater* **2016**, *15*, 896.
- (24) A. Hamidi-Sakr, L. Biniek, J.-L. Bantignies, D. Maurin, L. Herrmann, N. Leclerc, P. Leveque, V. Vijayakumar, N. Zimmermann and M. Brinkmann, *Advanced Functional Materials* **2017**, *27*, 1700173.
- (25) V. Vijayakumar, E. Zaborova, L. Biniek, H. Zeng, L. Herrmann, A. Carvalho, O. Boyron, N. Leclerc and M. Brinkmann, *ACS Appl. Mater. Interfaces* **2019**, *11*, 4942.
- (26) A. Hamidi-Sakr, L. Biniek, S. Fall and M. Brinkmann, *Advanced Functional Materials* **2016**, *26*, 408.
- (27) H. Kaneko and T. Ishiguro *Synth. Met.* **1994**, *65*, 141-148
- (28) Previous studies on FeCl₃-doped Polyacetylene (PA), have shown that the doping mechanism results in the formation of FeCl₄⁻ and FeCl₂ species following the reaction Polymer + 2 FeCl₃ → Polymer⁺ + FeCl₄⁻ + FeCl₂. H. Sakai, Y. Maeda, T. Kobayahi and H. Shirakawa, *Bull. Chem. Soc. Jpn*, **1983**, *56*, 1616.
- (29) N. C. Miller, E. Cho, R. Gysel, C. Risko, V. Coropceanu, C. E. Miller, S. Sweetnam, A. Sellinger, M. Heeney, I. McCulloch, J. L. Brédas, M. F. Toney and M. D. Mc Gehee, *Advanced Energy Materials* **2012**, *2*, 1208.
- (30) N. C. Miller, E. Cho, M. J. N. Junk, R. Gysel, C. Risko, D. Kim, S. Sweetnam, C. E. Miller, L. J. Richter, R. J. Kline, M. Heeney, I. McCulloch, A. Amassian, D. Acevedo-Feliz, C. Knox, M. R. Hansen, D. Dudenko, B. F. Chmelka, M. F. Toney, J.-L. Brédas and M. D. McGehee *Advanced Materials* **2012**, *24*, 6071.
- (31) B. – K. Yang, C.-A. Wang, W.-Y. Zhang, and J. Ruan, *J. Polym. Sci. B: Polym. Phys.* **2017**, *55*, 1448.
- (32) K. E. Aasmundtveit, E. J. Samuelsen, L. A. A. Pettersson, O. Inganäs, T. Johansson and R. Feidenhans'l, *Synthetic Metals* **1999**, *101*, 561.
- (33) E.-G. Kim and J.-L. Brédas, *J. Am. Chem. Soc.* **2008**, *130*, 16880.
- (34) E. Cho, C. Risko, D. Kim, R. Gysel, N. C. Miller, D. W. Breiby, M. D. McGehee, M. F. Toney, R. J. Kline, and J.-L. Brédas, *J. Am. Chem. Soc.* **2012**, *134*, 6177

- (35) A. Hamidi-Sakr, D. Schiefer, S. Covindarassou, L. Biniek, M. Sommer and M. Brinkmann, *Macromolecules* **2016**, 49, 3452.
- (36) B. McCulloch, V. Ho, M. Hoarfrost, C. Stanley, C. Do, W. T. Heller and R. A. Segalman, *Macromolecules* **2013**, 46, 1899.
- (37) L. H. Zhao and R. Q. Png, *Macromolecules* **2011**, 44, 9692.
- (38) J. Yamamoto and Y. J. Furukawa, *Phys. Chem. B* **2015**, 119, 4788.
- (39) J. Hwang, D. B. Tanner, I. Schwendeman and J. R. Reynolds, *Phys. Rev. B* **2003**, 67, 115205.
- (40) R. Ghosh, C. M. Pochas and F. C. Spano, *J. Phys. Chem. C* **2016**, 120, 11394.
- (41) R. Ghosh, A. R. Chew, J. Onorato, V. Pakhnyuk, C. K. Luscombe, A. Salleo, F. C. Spano, *J. Phys. Chem. C* **2018**, 122, 18048–18060.
- (42) H. Li, M. E. DeCoster, R. M. Ireland, J. Song, P. E. Hopkins and H. E. Katz, *J. Am. Chem. Soc.* **2017**, 139, 11149.
- (43) H. Tanaka, M. Hirate, S. Watanabe and S.-I. Kuroda *Adv. Mat.* **2014**, 26, 2376.
- (44) P. Sheng, *Phys. Rev. B* **1980**, 21, 2180.
- (45) F. J. Blatt, P. A. Schroeder, C. L. Foiles, D. Greig in *Thermopower of Metals*, Plenum Press, New York and London, **1976**, p. 5.
- (46) A. B. Kaiser, *Phys. Rev. B* **1989**, 40, 2806.
- (47) W. Pukacki, J. Plochanski and S. Roth, *Synthetic Met.* **1994**, 62, 253.
- (48) C. L. Choy, *Polymer* **1977**, 18, 984.
- (49) M. G. Kanatzidis, *Chem. Mater.* **2010**, 22, 648.
- (50) S. D. Kang and G. J. Snyder, *Nature Materials* **2016**, 16, 252
- (51) S. N. Patel, A. M. Glauddell, K. A. Peterson, E. M. Thomas, K. A. O'Hara, E. Lim and M. L. Chabinyk, *Science Advances* **2017**, 3, e1700434.
- (52) A. M. Glauddell, J. E. Cochran, S. N. Patel and M. L. Chabinyk, *Advanced Energy Materials* 2014, 5, 1401072.
- (53) N. Mateeva, H. Niculescu, J. Schlenoff and L. R. Testardi, *Journal of Applied Physics* **1998**, 83, 3111.
- (54) K. Tremel, F. S. U. Fischer, N. Kayunkid, R. Di Pietro, R. Tkachov, A. Kiriy, D. Neher, S. Ludwigs and M. Brinkmann, *Advanced Energy Materials* **2014**, 4, 1301659.
- (55) Y. Zhong, L. Biniek, N. Leclerc, S. Ferry and M. Brinkmann, *Macromolecules* **2018**, 51, 4238.

- (56) L. Biniek, A. Hamidi-Sakr, L. Grodd, S. Escoubas, Y. J. Dappe, S. Grigorian, M. Schmutz and M. Brinkmann, *Advanced Electronic Materials* **2018**, 4, 1700480.